A&A 384, 473–490 (2002)
DOI: 10.1051/0004-6361:20020032
© ESO 2002

Astronomy & Astrophysics

An atlas of 2.4 to 4.1 μm ISO/SWS spectra of early-type stars⋆,⋆⋆

A. Lenorzer[1], B. Vandenbussche[2], P. Morris[3], A. de Koter[1], T. R. Geballe[4], L. B. F. M. Waters[1,2], S. Hony[1], and L. Kaper[1]

[1] Sterrenkundig Instituut "Anton Pannekoek", Kruislaan 403, 1098 SJ Amsterdam
[2] Instituut voor Sterrenkunde, K. U. Leuven, Celestijnenlaan 200B, 3001 Heverlee
[3] SIRTF Science Center / IPAC, California Institute of Technology, M/S 100-22, 1200 E. California Blvd., Pasadena, CA 91125, USA
[4] Gemini Observatory, 670 N. A'ohoku Place, Hilo, HI 96720, USA

Received 10 October 2001 / Accepted 7 January 2002

Abstract. We present an atlas of spectra of O- and B-type stars, obtained with the Short Wavelength Spectrometer (SWS) during the Post-Helium program of the Infrared Space Observatory (ISO). This program is aimed at extending the Morgan & Keenan classification scheme into the near-infrared. Later type stars will be discussed in a separate publication. The observations consist of 57 SWS Post-Helium spectra from 2.4 to 4.1 μm, supplemented with 10 spectra acquired during the nominal mission with a similar observational setting. For B-type stars, this sample provides ample spectral coverage in terms of subtype and luminosity class. For O-type stars, the ISO sample is coarse and therefore is complemented with 8 UKIRT L'-band observations. In terms of the presence of diagnostic lines, the L'-band is likely the most promising of the near-infrared atmospheric windows for the study of the physical properties of B stars. Specifically, this wavelength interval contains the Brα, Pfγ, and other Pfund lines which are probes of spectral type, luminosity class and mass loss. Here, we present simple empirical methods based on the lines present in the 2.4 to 4.1 μm interval that allow the determination of *i)* the spectral type of B dwarfs and giants to within two subtypes; *ii)* the luminosity class of B stars to within two classes; *iii)* the mass-loss rate of O stars and B supergiants to within 0.25 dex.

Key words. line: identification – atlases – stars: early-type – stars: fundamental parameters – infrared: stars

1. Introduction

The advance of infrared-detector technology since the eighties has opened new perspectives for the study of early-type stars. Investigation of the early phases of their evolution especially benefits from infrared (IR) observations. The birth places of massive stars are identified with Ultra-Compact HII regions (UCHII). In such regions, the stars are still embedded in material left over from the star formation process and are obscured at optical and ultraviolet wavelengths. In the K-band (ranging from 2.0 to 2.4 μm) dust optical depths τ of a few occur, while in the H-band (ranging from 1.5 to 1.8 μm) τ is typically of order ten. At shorter wavelengths, the dust extinction becomes too high to observe the embedded stars. The IR emission of the warm dust cocoon covering the newly formed massive stars in UCHII regions peaks typically at about 100 μm. At wavelengths longwards of 5–10 μm, the thermal emission of the dust dominates the photospheric flux, and can be as much as 4 orders of magnitude above the stellar free-free continuum at 100 μm (Churchwell 1991).

Reliable values for the luminosities, temperatures and mass-loss rates of the embedded massive stars are essential as they allow us to trace the very early phases of their evolution of which little is known. Furthermore, these parameters control the photo-dissociation and ionisation of the molecular gas, the evaporation of the dust, and affect the morphology of the UCHII region.

The development of *quantitative* diagnostics based on IR spectral data requires, as a first step, homogeneous observations of a large set of both normal and peculiar non-embedded early-type stars, that have been studied in detail at optical and ultraviolet wavelengths where OB-type stars exhibit many spectral lines. Such stars may be used to calibrate quantitative methods based on IR spectroscopy alone. Calibration work has

Send offprint requests to: A. Lenorzer,
e-mail: lenorzer@astro.uva.nl

⋆ Based on observations with ISO, an ESA project with instruments funded by ESA Member States (especially the PI countries: France, Germany, The Netherlands and the UK) and with the participation of ISAS and NASA.

⋆⋆ The appendix is only available in electronic form at the CDS via anonymous ftp to cdsarc.u-strasbg.fr (130.79.128.5) or via
http://cdsweb.u-strasbg.fr/cgi-bin.qcat?J/A+A/384/473

Article published by EDP Sciences and available at http://www.aanda.org or http://dx.doi.org/10.1051/0004-6361:20020032

Table 1. The 12 O-type stars and one Wolf-Rayet star observed during the ISO/SWS Post-Helium mission, supplemented with 7 O stars observed with CGS4/UKIRT. The spectrum averaged signal-to-noise ratio (S/N) is listed in the last column.

Star	Name	Spectral Type	Spect. Type Reference[a]	ISO Observation Number	Instrument	S/N
HD 46223	NGC 2244 203	O4V((f))	W72		UKIRT	220
HD 190429A		O4If+	W73	89 300 401	ISO/PHe	15
HD 46150	NGC 2244 122	O5V(f)	W72		UKIRT	150
HD 199579	HR 8023	O6V((f))	W73	89 300 301	ISO/PHe	20
HD 206267	HR 8281	O6.5V((f))	W73	90 001 601	ISO/PHe	30
HD 47839	15 Mon	O7V((f))	W72		UKIRT	70
HD 24912	ζ Per	O7.5III((f))	W73		UKIRT	125
HD 188001	QZ Sge	O7.5Iaf	W72	90 000 801	ISO/PHe	10
HD 36861	λ Ori A	O8III((f))	W72		UKIRT	180
HD 209481	LZ Cep	O9V	W73	90 001 701	ISO/PHe	25
HD 193322	HR 7767	O9V((n))	W72	88 201 401	ISO/PHe	15
HD 37043	ι Ori	O9III	W72		UKIRT	140
HD 207198	HR 8327	O9Ib-II	W72	88 502 001	ISO/PHe	25
HD 38666	μ Col	O9.5V	W73	90 701 901	ISO/PHe	10
HD 37468	σ Ori	O9.5V	C71		UKIRT	165
HD 209975	19 Cep	O9.5Ib	W72	90 001 501	ISO/PHe	30
HD 188209	HR 7589	O9.5Iab	W72	88 000 501	ISO/PHe	20
HD 30614	α Cam	O9.5Ia	W72	88 300 601	ISO/PHe	85
HD 195592		O9.7Ia	W72	90 001 101	ISO/PHe	45
WR 147		WN8h	S96	88 000 701	ISO/PHe	35

[a] C71: Conti & Alschuler (1971); W72: Walborn (1972); W73: Walborn (1973); S96: Smith et al. (1996).

already been carried out in other near-infrared wavelength ranges, in the J-band by e.g. Wallace et al. (2000), in the H-band by e.g. Meyer et al. (1998) and Hanson et al. (1998), and in the K-band Hanson et al. (1996). The "Post-Helium program" conducted with the Short Wavelength Spectrometer (SWS) on board the Infrared Space Observatory (ISO) is intended to provide such a data set. This mission started after helium boil-off in April 1998 and made use of the ability of the detectors of SWS to acquire observations in band 1 [2.4–4.1] μm during the slow warming of the satellite (see also Sect. 2.1). The band 1 of ISO SWS ranges from 2.4 to 4.1 μm, and is, like the K-band, positioned favourably in the narrow window in which newly born stars can be observed directly. This wavelength region contains important diagnostic hydrogen lines of the Brackett (Brα, Brβ), Pfund (Pfγ), and Humphreys series.

In this paper, we present and study 75 spectra of early-type stars, 67 [2.4–4.1 μm] ISO/SWS spectra and 8 [3.5–4.1 μm] spectra observed with the United Kingdom Infrared Telescope (UKIRT). This sample includes OB, Be, and Luminous Blue Variable (LBV) stars. We discuss line trends as a function of spectral type, following a strategy similar to the one adopted by Hanson et al. (1996) for the K-band. Simple empirical methods are employed to derive the spectral type and/or luminosity class. These methods may also be applied if only ground-based L'-band spectra are available (which cover a smaller wavelength range).

The paper is organised as follows: in Sect. 2 we discuss the data acquisition and reduction techniques; Sect. 2.3 comprises a catalogue of good quality spectra; Sect. 3 provides the line identifications. Line trends and methods to classify OB-type stars are presented in Sect. 4, while Sect. 5 describes the spectra of B stars with emission lines. The results are summarised in the final section. The equivalent-width measurements are listed in the Appendix.

2. Observations

2.1. The ISO/SWS sample

The ISO spectra were obtained with ISO/SWS (SWS, de Graauw et al. 1996; ISO, Kessler et al. 1996). After helium boil-off of the ISO satellite on 8 April 1998, the near-infrared band 1 [2.4–4.1 μm] of SWS equipped with InSb detectors could still be operated as the temperature at the focal plane increased only slowly. Between 13 April and 10 May, spectra of nearly 250 bright stars were acquired for a stellar classification program. Referred to as "Post-Helium observations", this program aims at extending the MK classification scheme into the near-infrared.

In this paper we present the subset of O- and B-type stars observed during the Post-Helium phase. These observations were executed using a dedicated engineering observation mode, the so-called Post-Helium observation template. All the spectra obtained during the Post-Helium program, including later spectral types, as well as details about the data acquisition will be published in a separate publication (Vandenbussche et al. in prep). Along with these Post-Helium spectra, we include ten spectra of O and B stars measured during the nominal mission using Astronomical Observation Template 1 speed 4 [AOT01].

Table 2. The 30 B-type stars observed during the ISO/SWS Post-Helium mission, supplemented with 3 stars from the ISO/SWS nominal mission and 1 star observed with CGS4/UKIRT.

Star	Name	Spectral Type	Spect. Type Reference[a]	ISO Observation Number	Instrument	S/N
HD 202214	HR 8119	B0V	M55	90 300 701	ISO/PHe	15
HD 93030	θ Car	B0Vp	B62	25 900 905	ISO/Nom	115
HD 37128	ϵ Ori	B0Ia	W90		UKIRT	115
HD 198781	HR 7993	B0.5V	M55	88 301 201	ISO/PHe	10
HD 207793		B0.5III	M55	88 700 901	ISO/PHe	20
HD 185859	HR 7482	B0.5Ia	M55	89 901 301	ISO/PHe	6
HD 116658	α Vir	B1V	M55	25 302 001	ISO/Nom	165
HD 208218		B1III	M55	88 701 101	ISO/PHe	7
HD 190066		B1Iab	M55	88 101 401	ISO/PHe	15
HD 158926	λ Sco	B1.5IV	H69	49 101 016	ISO/Nom	140
HD 52089	ϵ Cma	B1.5II	W90	88 602 001	ISO/PHe	130
HD 194279	V2118 Cyg	B1.5Ia	L92	88 201 301	ISO/PHe	80
HD 193924	α Pav	B2IV	L75	88 500 501	ISO/PHe	95
HD 206165	9 Cep	B2Ib	L68	88 300 301	ISO/PHe	70
HD 198478	55 Cyg	B2.5Ia	L68	88 100 501	ISO/PHe	100
HD 160762	ι Her	B3V	J53	89 900 101	ISO/PHe	70
HD 207330	π^2 Cyg	B3III	M55	88 701 301	ISO/PHe	45
HD 15371	κ Eri	B5IV	H69	90 701 401	ISO/PHe	35
HD 184930	ι Aql	B5III	L68	88 000 901	ISO/PHe	45
HD 191243	HR 7699	B5II	L92	88 401 401	ISO/PHe	20
HD 58350	η Cma	B5Ia	W90	90 702 301	ISO/PHe	90
HIC 101364	Cyg OB2 12	B5Ia	M91	90 300 901	ISO/PHe	105
HD 203245	HR 8161	B6V	L68	88 701 401	ISO/PHe	10
HD 155763	ζ Dra	B6III	L68	89 900 201	ISO/PHe	80
HD 209952	α Gru	B7IV	H69	88 500 701	ISO/PHe	150
HD 183143	HT Sge	B7Ia	M55	89 901 501	ISO/PHe	60
HD 14228	ϕ Eri	B8V-IV	H69	88 701 901	ISO/PHe	75
HD 207971	γ Gru	B8III	H82	88 500 901	ISO/PHe	100
HD 208501	13 Cep	B8Ib	L92	88 701 201	ISO/PHe	80
HD 199478	V2140 Cyg	B8Ia	L92	88 501 801	ISO/PHe	60
HD 16978	ϵ Hyi	B9V	H75	88 401 901	ISO/PHe	65
HD 196867	α Del	B9IV	M73	88 101 701	ISO/PHe	75
HD 176437	γ Lyr	B9III	J53	88 401 501	ISO/PHe	110
HD 202850	σ Cyg	B9Iab	M55	90 600 601	ISO/PHe	65

[a] J53: Johnson & Morgan (1953). M55: Morgan et al. (1955), B62: Buscombe (1962), L68: Lesh (1968), H69: Hiltner et al. (1969), M73: Morgan & Keenan (1973), L75: Levato (1975), H75: Houk (1975), H82: Houk (1982), W90: Walborn & Fitzpatrick (1990), M91: Massey & Thompson (1991), L92: Lennon et al. (1992).

Both observation templates use the same scanning strategy, SWS takes a full continuous spectrum over four preset overlapping sub-bands. These are defined in Table 4. The integration time per target is fixed, therefore the S/N ratio mainly depends on the brightness of the source.

Combining the nominal and Post-Helium program AOT01 speed 4 observations, we collected 69 ISO/SWS spectra. However, two targets (HD 147165 and HD 203245) were clearly off-pointed and will therefore not be discussed. We split the remaining 67 stars into two subgroups: the O- and B-type stars, and the B stars with emission-line spectra. Spectra over 2.4–4.1 μm for the majority of these stars are presented for the first time. For comparison with Of supergiants, we have included the Wolf-Rayet star WR 147 (Van der Hucht et al. 1996) in the first subgroup. The second subgroup includes 18 Be and 3 Luminous Blue Variable (LBV) stars (see Humphreys & Davidson 1994 for a review). Spectra of AG Car and P Cyg have been presented by Lamers et al. (1996a,b). The 45 OB stars are listed in Tables 1 and 2 together with 8 OB stars observed with UKIRT; the 21 B stars with emission lines are given in Table 3.

Each table provides the HD number and stellar name; the spectral type and luminosity class; the ISO/SWS observation number and a label indicating whether the observation was done during the nominal or Post-Helium program, quoted by the acronym ISO/Nom and ISO/PHe, respectively. The last column provides a spectrum averaged value of the signal-to-noise ratio (S/N) of the observation (see Sect. 2.1.1). On average the S/N is relatively low for the O- and early B-type stars: only 5 out of 22 stars

Table 3. The 14 B stars with emission lines observed in the ISO/SWS Post-Helium mission supplemented with 7 stars observed during the ISO/SWS nominal mission.

Star	Name	Spectral Type	Spect Type Reference[a]	Observation Number	Status	S/N
V1478 Cyg	MWC 349A	O9III[e]	Z98	18 500 704	ISO/Nom	145
HD 206773	MWC 376	B0Vpe	M55	88 502 101	ISO/PHe	20
HD 5394	γ Cas	B0.5Ve	P93	24 801 102	ISO/Nom	150
HD 212571	π Aqr	B1Ve	L68	90 601 301	ISO/PHe	20
HD 50013	κ Cma	B1.5IVne	H69	90 702 001	ISO/PHe	80
HD 200775	MWC 361	B2V[e]	G68	90 300 501	ISO/PHe	50
HD 45677	MWC 142	B2V[e]	Z98	71 101 992	ISO/Nom	135
HD 56139	ω Cma	B2IV-Ve	H69	90 702 201	ISO/PHe	40
HD 105435	HR 4621	B2IVne	H69	07 200 272	ISO/Nom	120
HD 205021	β Cep	B2IIIe	M55	88 100 301	ISO/PHe	110
HD 187811	12 Vul	B2.5Ve	L68	90 700 901	ISO/PHe	25
HD 191610	28 Cyg	B2.5Ve	L68	89 900 901	ISO/PHe	35
HD 205637	ϵ Cap	B3Vpe	H88	90 601 701	ISO/PHe	30
HD 10144	α Eri	B3Vpe	H69	90 000 101	ISO/PHe	140
HD 56014	EW Cma	B3IIIe	H82	90 702 101	ISO/PHe	20
HD 50123	HZ Cma	B6Vnpe	S	88 601 901	ISO/PHe	75
HD 198183	λ Cyg	B6IVe	L68	89 900 801	ISO/PHe	35
HD 209409	omi Aqr	B7IVe	L68	90 601 501	ISO/PHe	35
HD 193237	P Cygni	B2pe	L68	33 504 020	ISO/Nom	100
HD 94910	AG Car	B2pe	H75	22 400 153	ISO/Nom	80
HD 93308	η Car	Bpe	H75	07 100 250	ISO/Nom	170

[a] M55: Morgan et al. (1955), L68: Lesh (1968), G68: Guetter (1968), H69: Hiltner et al. (1969), H75: Houk (1975), H82: Houk (1982), H88: Houk (1988), P93: van Paradijs (1993), Z98: Zorec et al. (1998), S: Simbad.

Table 4. The spectral resolution R and wavelength coverage of the four sub-bands, for a detailed technical specification see de Grauw et al. (1996).

preset sub-band	$R = \Delta\lambda/\lambda$	wavelength coverage (μm)
band 1a	1870–2110	2.38–2.60
band 1b	1470–1750	2.60–3.02
band 1d	1750–2150	3.02–3.52
band 1e	1290–1540	3.52–4.08

of spectral type earlier than B2 have a $S/N \geq 60$; for the later type stars the situation is reversed, i.e. only 5 out of 23 have $S/N \leq 60$. This tendency is explained by the lack of relatively nearby bright O and early-B stars compared to later B stars. For the B stars with emission lines, the S/N of the continuum is not that important as the emission lines are very prominent in most of the spectra.

The 34 B stars provide a fairly dense coverage of B spectral types, but this is not the case with the 12 O stars. Moreover, because of the relatively low S/N of our observations, we could not detect lines in any of the five O V stars. Lines are detected, however, in supergiant O stars. We obtained L'-band UKIRT observations in order to improve the coverage of O spectral types. These are discussed in Sect. 2.2. The subgroup of B stars with emission-line spectra shows a diversity in the way their circumstellar material is distributed: 18 Be stars with discs and/or shells and 3 LBV stars (η Carinae, AG Carinae and P Cygni) with dense stellar winds.

2.1.1. ISO/SWS data reduction

The data acquired during the nominal mission were calibrated in the SWS Interactive Analysis environment with the calibration files as in Off-Line Processing Version 10.0. The Post-Helium data required special care as changes in the characteristics of the instrument arose when the temperature increased. A time-dependent calibration was derived, based on reference observations in each orbital revolution of the satellite. This accounts for changes in wavelength calibration and photometric sensitivity as a function of wavelength. Fortunately, the spectral resolution did not change and the dark current and noise remained fairly similar, as the signal registered with closed instrument shutter is still dominated by the amplifier offsets. The exact sources of instrumental drifts cannot be fully disentangled but a reliable empirical calibration could be derived. The Post-Helium calibration, which is described in detail in Vandenbussche et al. (2000), results in a data quality that is comparable to that during the nominal mission. To illustrate this: P Cyg was observed both during the nominal and Post-helium missions, the spectra show a continuum level variation of 4% and a line width variation of 5%.

All the spectra were processed from the Auto-Analysis Result stage using the SWS Interactive Analysis (IA^3) programs. First, the behaviour of the individual detectors was checked. Second, the two independent spectral scans were compared. Discrepancies were treated when

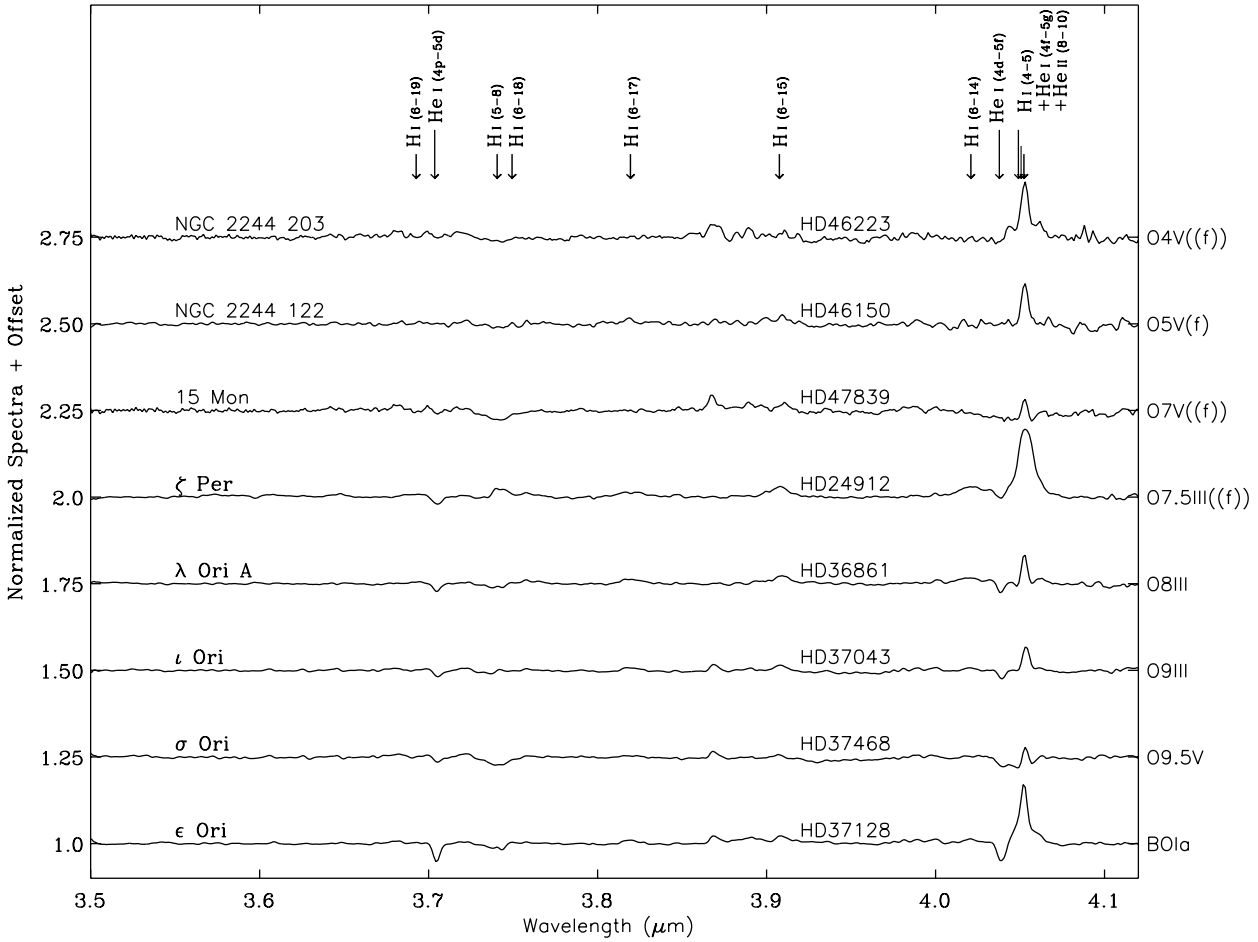

Fig. 1. The 3.5 to 4.12 μm region of the spectra of O- type stars obtained with CGS4/UKIRT. All O stars in this sample show Brα emission in the core.

their cause was clearly established (jumps, glitches, residual tilt in the slope of the Post-Helium spectra). The adopted spectral resolution per sub-band is very similar to the R values given in Sect. 2.1, but not strictly identical, as the final rebinning is based on on-board measurements (see Lorente et al. 1998; Hony et al. 2000).

2.2. The CGS4/UKIRT sample

The UKIRT spectra were obtained on the second half of the night of 23 December 2000 (UT) using the Cooled Grating Spectrometer 4 (CGS4; Mountain et al. 1990). We obtained L'-band (3.5–4.1 μm) spectra of 8 stars with spectral types ranging from O4 to B0. The 40 l/mm grating was used in first order with the 300 mm focal length camera and the 0.6″ wide slit, giving a nominal resolution of 0.0025 μm ($R \approx 1500$). The array was stepped to provide 2 data points per resolution element. Signal-to-noise ratios of 70 to 200 were achieved on the continua of the target hot stars. The four O V stars, with subtypes O4, O5, O7, and O9.5 significantly improve the coverage of spectral types. Three O7 to O9 giants were also observed, as well as one B0 supergiant.

For data reduction, we used the Starlink Figaro package. Spectra were ratioed by those of dwarf A and F stars observed on the same night at similar airmasses as the hot stars, corrected for the approximate effective temperatures of the stars by multiplying by a blackbody function. Wavelength calibration was achieved using the second order spectrum of an argon arc lamp. The spectra shown here have been slightly smoothed, and have a resolution of 0.0031 μm ($R \approx 1200$).

2.3. Atlas

We present the normalised ISO/SWS spectra of O and B stars with S/N greater than 30 from 2.6 to 3.35 μm and from 3.65 to 4.08 μm in Figs. 2 to 4. We do not display the band 1a (from 2.4 to 2.6 μm) because the S/N of this sub-band, containing the higher Pfund series and for two stars only a probable Si IV line, is significantly lower than for the others. The spectra from 3.35 to 3.65 μm do not show any detectable lines. Figure 1 displays the L'-band spectra obtained with CGS4/UKIRT. Figures 5 and 6 display the full ISO/SWS band 1 spectra of all Be and Luminous Blue Variables stars in our sample. Line identifications are provided in each of the figures.

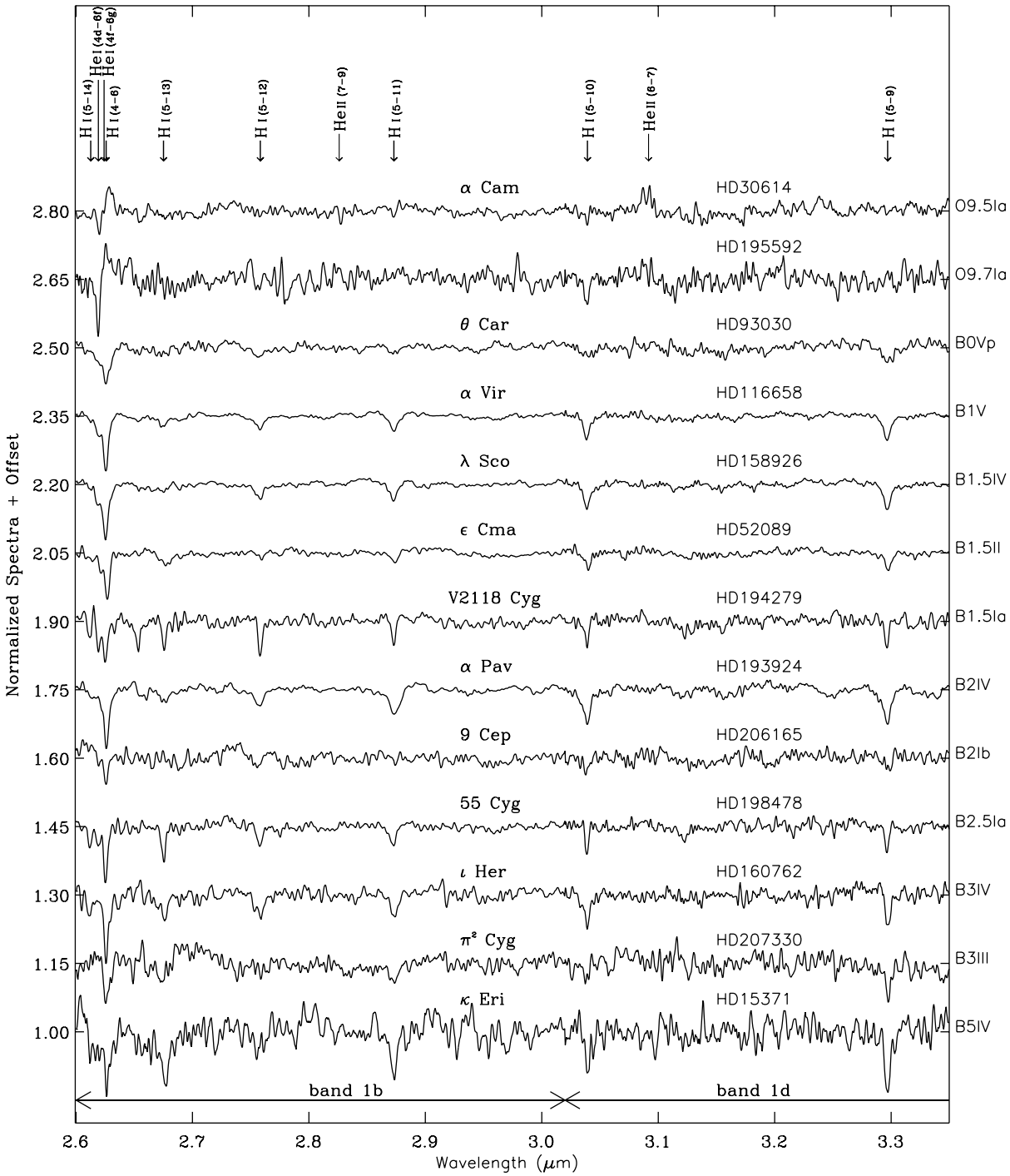

Fig. 2. The 2.6 to 3.35 μm region of the spectra of O9- to B5-type stars contains the Brβ line at λ 2.6259 μm and some of the Pfund series lines. A few helium lines are detected in the hottest stars and are identified with arrows in the top of the figure. The O supergiants show Brβ emission.

3. Identification and measurement of spectral lines

In this section, we give an overview of the lines observed in the 2.4 to 4.1 μm region and review how we measured line strengths and widths. The investigated spectral range is dominated by lines of hydrogen and helium. We made a special effort to identify lines of other elements, resulting in the detection of only one silicon emission line in two late O supergiants and a few lines of oxygen, magnesium and iron, in the sample of B stars with emission lines.

3.1. Overview of lines in the 2.4 to 4.1 μm region

Hydrogen lines of three different series are present in this wavelength region: the two leading lines of the Brackett series Brα λ4.0523 (wavelength in μm) and Brβ λ2.6259;

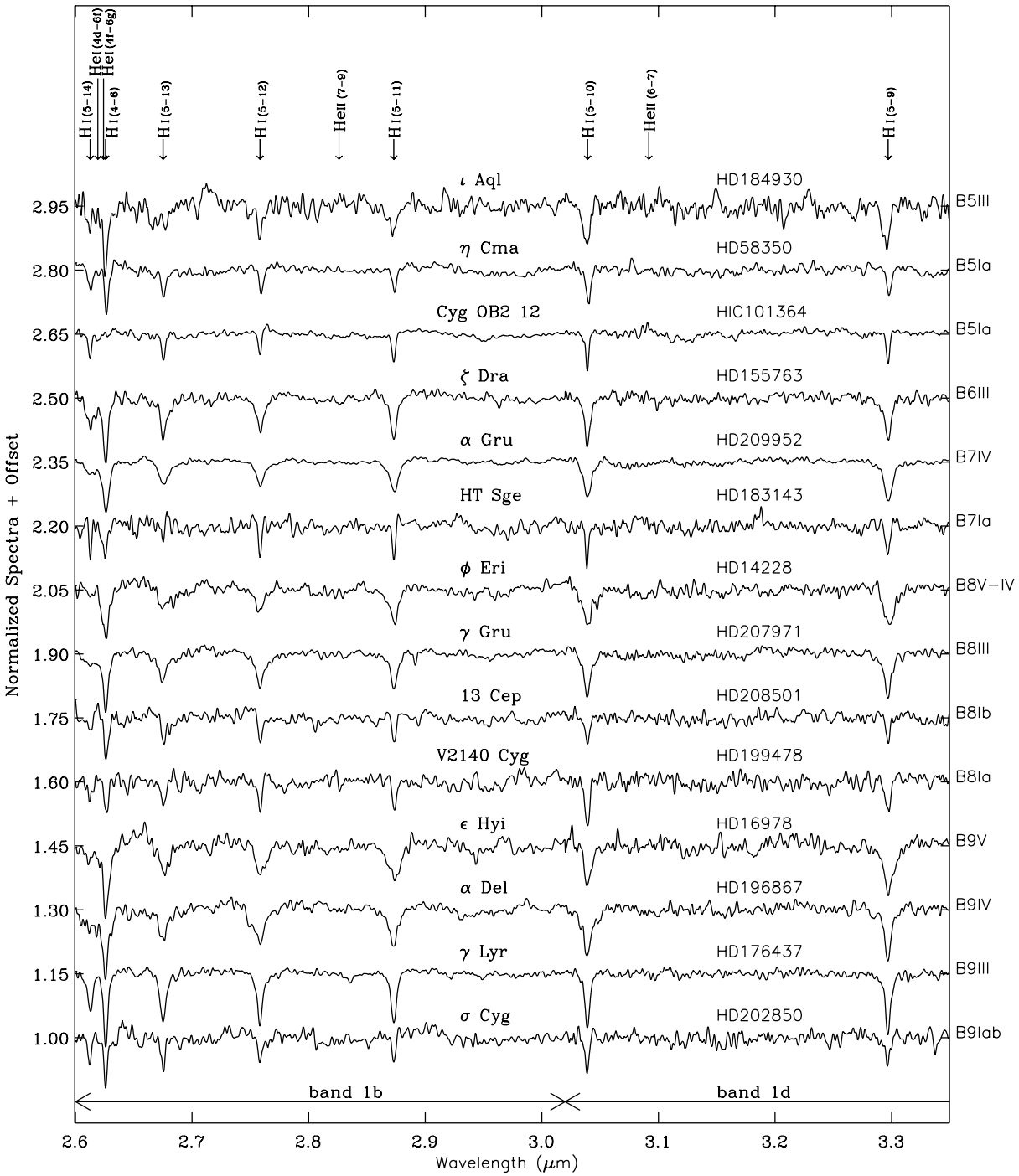

Fig. 3. The 2.6 to 3.35 μm region of the spectra of B5- to B9-type stars contains the Brβ line at λ 2.6259 μm and some lines of the Pfund series. Helium lines are no longer present.

the Pfund series from Pfγ λ3.7406 to Pf(22–5) λ2.4036, and the higher members of the Humphreys series starting from transition Hu(14–6) λ4.0209. The lower members of each series, such as Brα, Brβ and Pfγ, are expected to be particularly important diagnostic lines.

Lines of ionised helium are identified in three O supergiant stars. The (7–6) transition at λ3.0917 is expected to be the strongest He II line in the H, K and L'-bands. A second strong He II line, (9–7) at λ2.8260, is detected in the spectrum of the early-O supergiant HD 190429 and possibly in HD 188001 and HD 30614. It is likely that He II (10–8), (11–8) and (12–8) are present in the spectrum of HD 190429 based on a comparison with WR 147, but as these lines are located in the wings of the much stronger Brα, He II (7–6) and Brβ lines, respectively, we cannot provide a positive identification.

The neutral helium line that is expected to be the strongest is He I (5d–4f) at λ4.0490. Unfortunately, this line is blended with Brα. The second strongest He I line in band 1 is the (5f–4d) transition at λ4.0377. This line

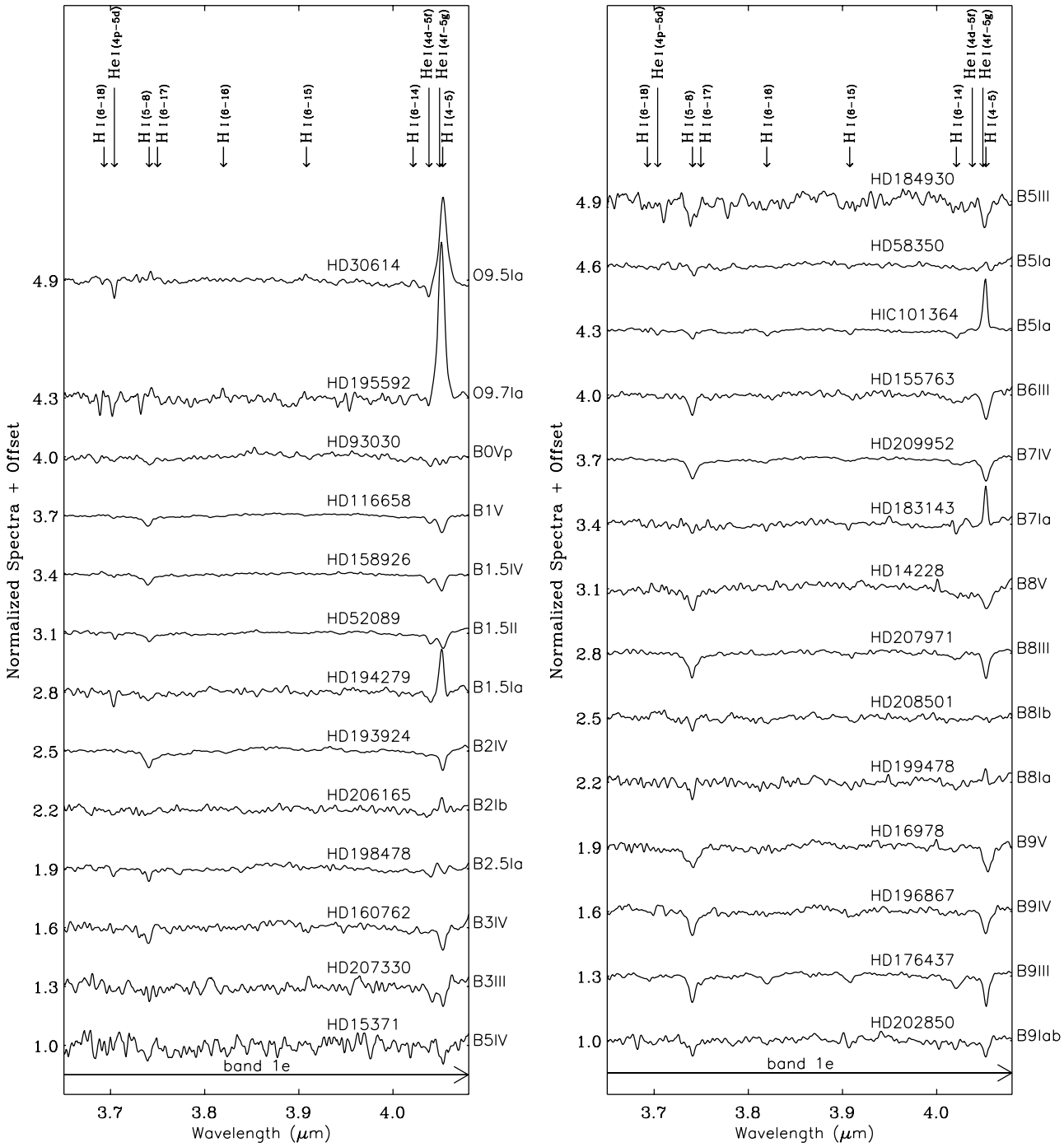

Fig. 4. The 3.65 to 4.08 μm region of the spectra of O9- to B9-type stars contains the Brα line at λ 4.0523 μm and some of the Humphreys series lines. He I lines are present down to spectral type B3 and are identified with arrows in the top of the figure. The OB supergiants show Brα emission down to B7/8.

is observed in absorption in stars from spectral type O9.5 down to B2.5 and in emission in Be stars of similar spectral type. Of comparable strength are He I (5d–4p) λ3.7036 and (6f–4d) λ2.6192. One would also expect, He I (6g–4f) λ2.6241, but this line is blended with Brβ and could not be detected.

We found an emission line at λ2.4275 in the two good quality spectra of the late-O supergiants HD 30614 and HD 195592, the most likely identification being Si IV(4f–4d). A few permitted O I as well as Fe II and likely Mg II lines could be identified in several Be stars and/or LBVs. Fe II (4s–4p) at λ3.0813, λ3.5423 and λ3.9378 is present in all three LBVs as well as in a few Be stars. Mg II (5p–4p) at λ2.4048 and λ2.4131 is possibly identified in all three LBVs. These identifications are consistent with the K-band spectra for the same stars, see

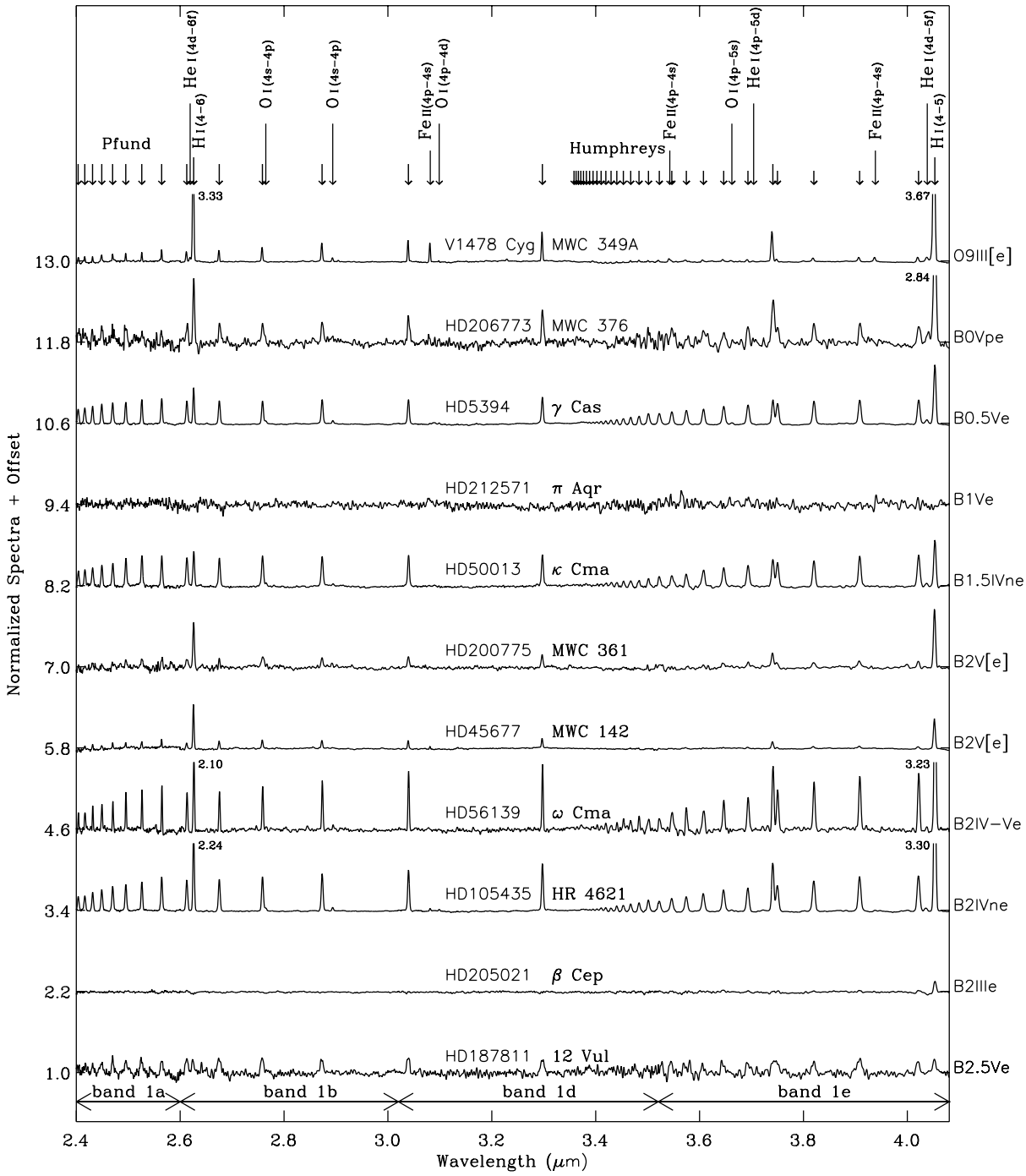

Fig. 5. The full band 1 spectra from 2.40 to 4.08 μm of B0e to B2.5e stars contain hydrogen lines of the Brackett, Pfund and Humphreys series. In most of the spectra, the only He I line present is at λ4.0377. A few stars also show some O I lines.

Hanson et al. (1996). Finally, four neutral oxygen lines are seen in early Be stars as well as in two LBVs: O I (4p–4s) at λ2.764 and λ2.893, O I (5s–4p) at λ3.662 and O I (4d–4p) at λ3.098. All identified lines are listed in Table 5.

A few forbidden lines are also observed in the spectra of LBV's and WR. We did not investigate those lines here, a listing of those can be found in Lamers et al. (1996b) and Morris et al. (2000).

3.2. Of supergiants and WR 147

The spectra of the two Of supergiants in our sample are plotted in Fig. 7 together with the spectrum of the Wolf-Rayet star WR 147. The ISO/SWS spectrum of WR147 has been analysed in detail by Morris et al. (2000). The line strengths in the Of spectra are significantly less than in the spectrum of WR 147, which is mainly a result of the

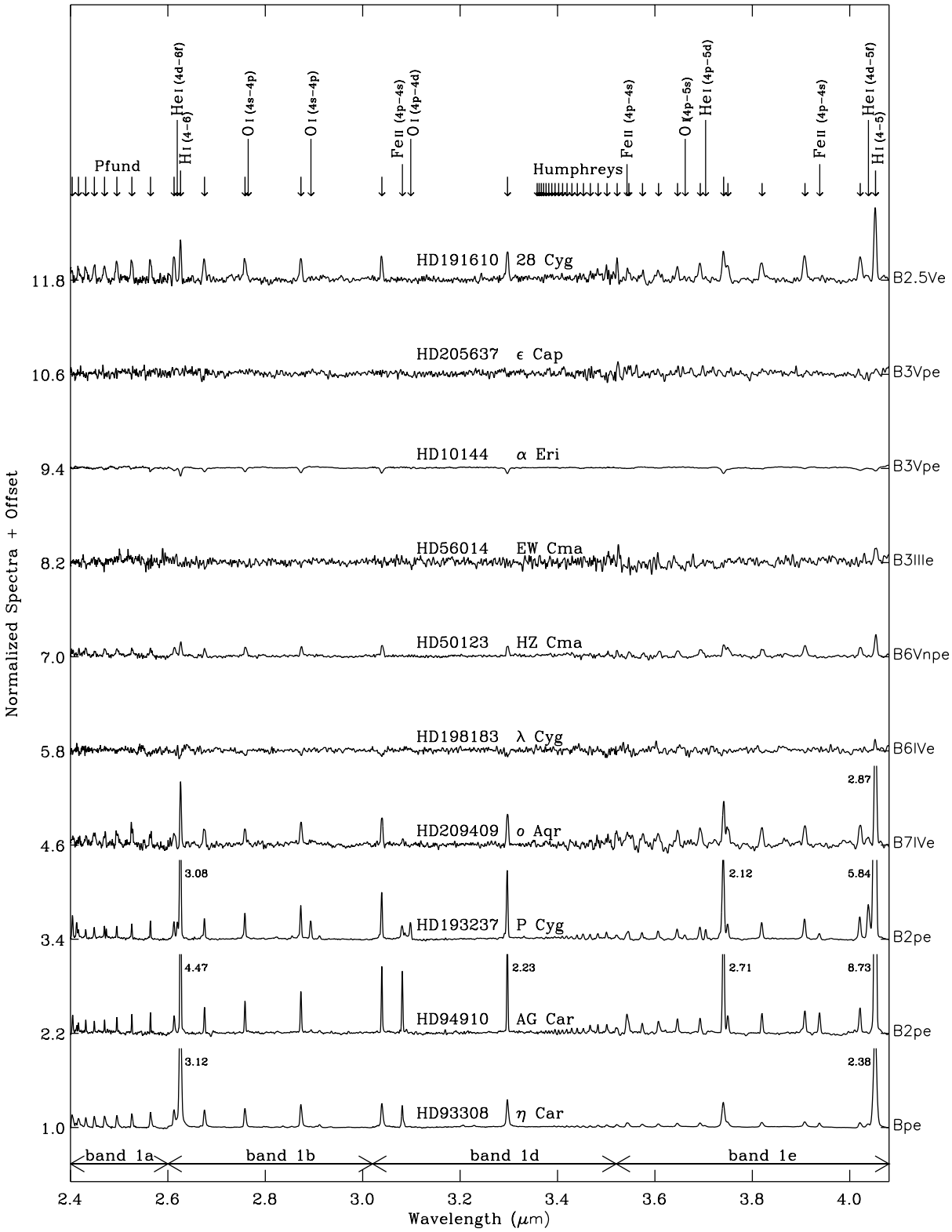

Fig. 6. The full band 1 spectra from 2.40 to 4.08 μm of B3e to B7e stars contain only hydrogen lines. HD 10144 does not currently show emission lines in its spectrum. The three Luminous Blue Variables, as well as the three peculiar Bpe stars, show some lines of He I, Fe II, Mg II and O I.

higher density of the wind of the Wolf-Rayet star. Line ratios such as Brβ/Brα and Pfα/Brα are roughly similar for both the Of stars and the WN8h, indicating the primary dependence of the line on mass flux $\dot{M}/4\pi R_\star^2$. However, the He II (7–6)/Brα line in HD 190429 is stronger by a factor of three compared to WR 147, indicating that this

Table 5. Lines identified in the [2.4–4.1] μm region.

λ_{vac} (μm)	Element	Configuration	λ_{vac} (μm)	Element	Configuration	λ_{vac} (μm)	Element	Configuration
2.404	H I	5–22	2.826	He II	7–9	3.546	H I	6–22
2.405	Mg II	4d–5p	2.873	H I	5–11	3.574	H I	6–21
2.413	Mg II	4d–5p	2.893	O I	$2s^2 2p^3 4s$–$2s^2 2p^3 4p$	3.607	H I	6–20
2.416	H I	5–21	3.039	H I	5–10	3.646	H I	6–19
2.427	Si IV	4d–4f	3.081	Fe II	$3d^6 4p$–$3d^6 4s$	3.662	O I	$2s^2 2p^3 4p$–$2s^2 2p^3 5s$
2.431	H I	5–20	3.092	He II	6–7	3.693	H I	6–18
2.449	H I	5–19	3.095	He II	8–11	3.704	He I	1s4p–1s5d
2.450	H I	5–18	3.098	O I	$2s^2 2p^3 4p$–$2s^2 2p^3 4d$	3.741	H I	5–8
2.473	He I	1s4p–1s6d	3.297	H I	5–9	3.749	H I	6–17
2.495	H I	5–17	3.402	H I	6–32	3.819	H I	6–16
2.526	H I	5–16	3.410	H I	6–31	3.907	H I	6–15
2.564	H I	5–15	3.419	H I	6–30	3.938	Fe II	$3d^6 4p$–$3d^6 4s$
2.613	H I	5–14	3.429	H I	6–29	4.021	H I	6–14
2.620	He I	1s4d–1s6f	3.440	H I	6–28	4.038	He I	1s4d–1s5f
2.624	He I	1s4f–1s6g	3.453	H I	6–27	4.041	He I	1s4d–1s5f
2.625	He II	8–12	3.467	H I	6–26	4.049	He I	1s4f–1s5g
2.626	H I	4–6	3.483	H I	6–25	4.051	He II	8–10
2.675	H I	5–13	3.501	H I	6–24	4.052	H I	4–5
2.758	H I	5–12	3.522	H I	6–23			
2.765	O I	$2s^2 2p^3 4s$–$2s^2 2p^3 4p$	3.542	Fe II	$3d^6 4p$–$3d^6 4s$			

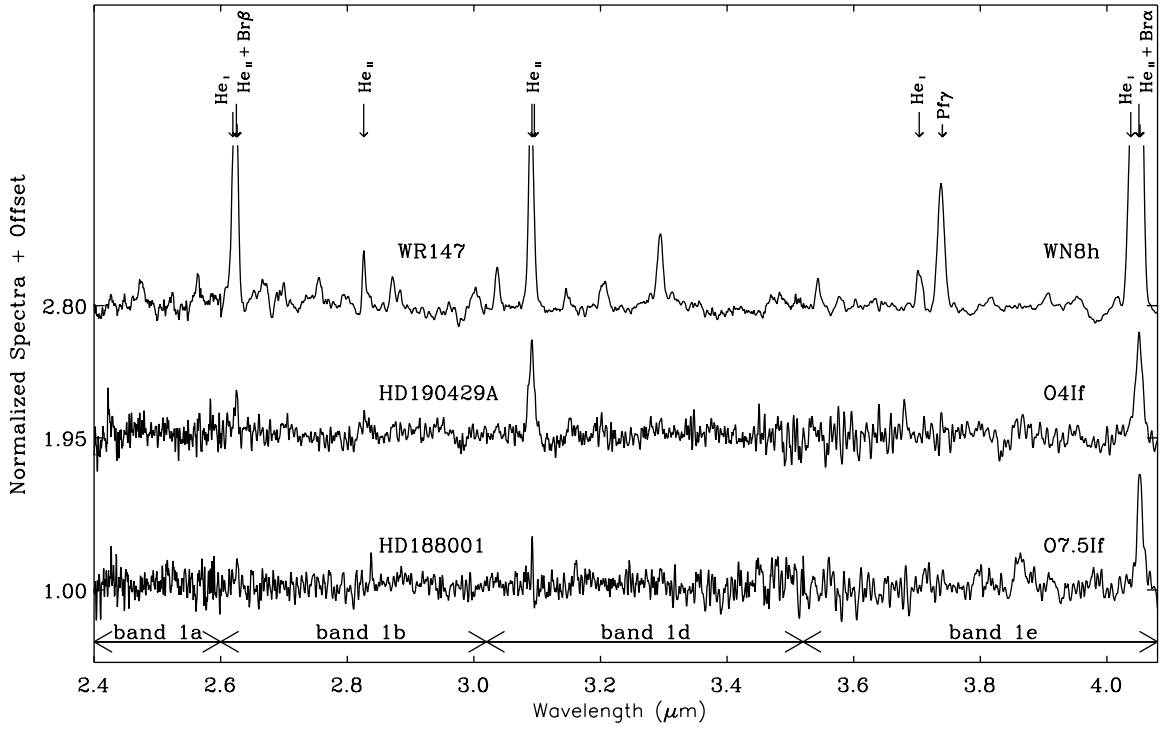

Fig. 7. Comparison of H I and He II lines between early Of-type supergiants and WR 147 in the 2.4 to 4.1 μm region. Line ratios such as Brβ/Brα and Pfγ/Brα are roughly similar; however He II (7–6) λ3.092/Brα in HD 190429 is stronger by a factor of three compared to WR 147, being consistent with the higher temperature of the O4If star (see Conti & Underhill 1988).

O4 star is significantly hotter. The higher temperature of the O4f stars is also implied by the absence of He I lines. A distinction between these types seems possible on the basis of overall line strength of the spectra (cf. Morris et al. 1997), though further investigation of WR spectral characteristics in the near-infrared is still needed to more firmly establish Of/WN differences (as in the K-band study of "transition" spectra by Morris et al. 1996) and connections.

Concerning the O7.5 If star, the Brackett lines are weaker and narrower than in the O4 If star indicating a lower mass-loss rate. Again, we do not detect He I lines;

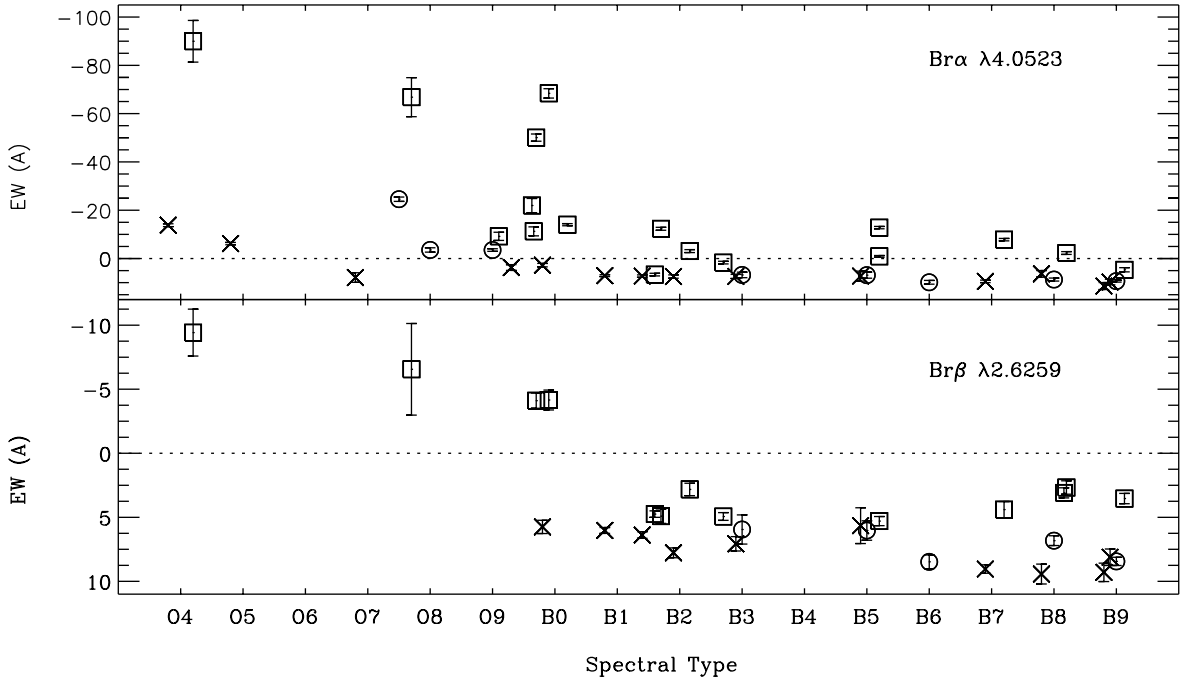

Fig. 8. The equivalent widths of Brα (top panel) and Brβ (bottom panel) for normal B-type stars. Stars of luminosity classes Ia-II are denoted by square symbols; class III by circles, and classes IV-V by crosses. The dotted lines indicate where the lines revert from absorption ($W_{\rm eq} > 0$) to emission ($W_{\rm eq} < 0$). For both lines, the B dwarfs and sub-giants show a gradual increase in absorption strength towards later spectral type. This can not be seen clearly in this figure, however the linear fit parameters of this trend are given in Table 6. In B supergiants and bright giants the line strength remains about constant, albeit with a large scatter.

the narrow feature at the position of the He II lines might be spurious. All other features between 3.4 and 4.0 μm are due to noise.

3.3. Equivalent width

For consistency in the measurements of equivalent widths, we first rebin the UKIRT spectra to the resolution of ISO/SWS. We then define the continuum regions after removing all the spectral sections containing identifiable lines. A normalisation function of the form $A_0 + A_1 \times X + A_2 \times X^{A_3}$ is fitted to each of the 4 sub-bands. The S/N is computed as being the inverse of the standard deviation on the normalised continuum. The line parameters, equivalent width (EW) and full width at half maximum ($FWHM$) are measured on the normalised spectra using the ISO Spectral Analysis Package. The errors on those measurements are dominated by the uncertainty in the position of the continuum, which is $\sim$5% (Decin et al. 2000). For unblended lines, the tool MOMENT is used as it gives statistical parameters without making any assumptions on the shape of the profile.

The signal-to-noise ratio and the spectral resolution of the ISO/SWS sample may vary over the spectrum (up to 50%), as well as within a sub-band. This is largely intrinsic to the instrument setting and depends little on the difference in flux over wavelengths; the S/N varies inversely to the spectral resolution.

The EWs of the lines used in our analysis (see Sect. 4) are presented in the Appendix. Concerning the O and B stars, this includes lines from all spectra that have $S/N \geq 35$. For a few bright giant and supergiant O-stars with signal-to-noise ratios smaller than this value, line measurements are presented for the relatively strong Brα profile, and in the case of HD 190429 (O4I) and QZ Sge (O7.5Ia) for the Brβ and He II (6–7) and (7–9) transitions. For one B star, HD 191243 (B5II), only three Pfund series lines could be measured. This is due to a poorer S/N of sub-band 1a compared to sub-bands 1b and 1d.

In the Be and LBV subgroups, lines could be measured with sufficient accuracy in all but two stars, ϵ Cap (B2.5Vpe) and π Aqr (B1Ve). The S/N of those two observations is quite low, 30 and 20, respectively, and the lines are not sufficiently prominent to be detectable in our ISO/SWS spectra.

4. Line trends and spectral classification of O and B stars

In discussing the trends in line strengths of O and B stars we separately consider luminosity classes Ia-II and III-V, because the behaviour of the hydrogen lines in the two groups is different. The difference is almost certainly connected to the density of the stellar wind. In main-sequence stars, which have weak winds, the line strength is dominated by temperature effects. As in optical spectra, one expects a gradual weakening of the lines towards higher

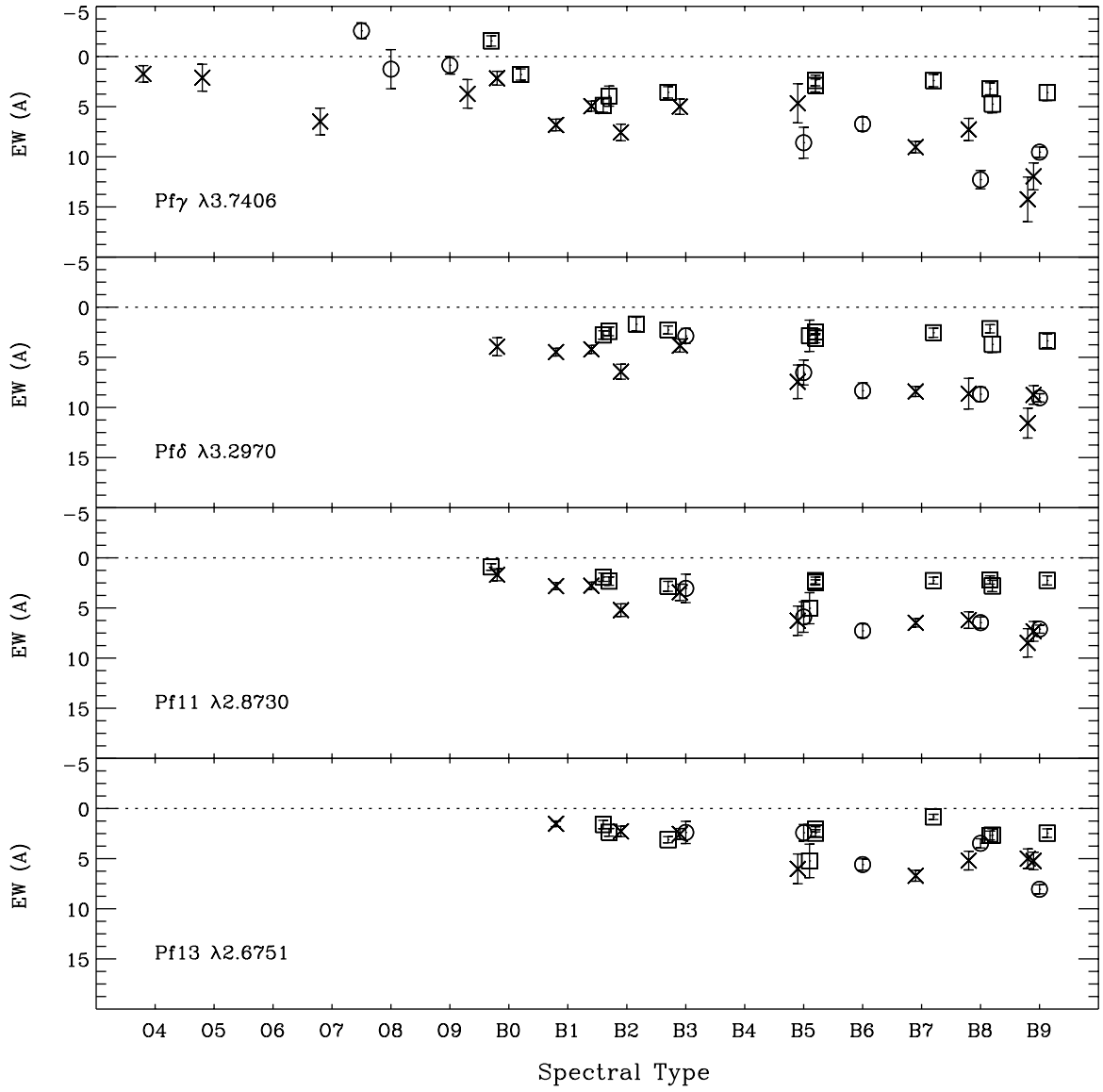

Fig. 9. The equivalent widths of four Pfund series lines for normal O and B-type stars. The symbols have identical meaning as in Fig. 8. Like the Bracket series lines, these Pfund lines show a different behaviour for B stars of luminosity classes Ia-II compared to classes IV-V, i.e. the latter show a gradual increase in absorption strength towards later spectral type, while in the former the strength remains about constant.

effective temperatures. In supergiant stars, which have dense winds, the strength of the lines connecting lower levels of a series (such as Brα) are expected to be highly sensitive to the stellar mass-loss rate $\dot{M}$, or better stated, to the stellar mass flux $\dot{M}/4\pi R_\star^2$. Indeed, in our data set Brα reverts from a strong absorption profile in B giants and dwarfs to a strong emission profile in B supergiants, suggesting that the line is sensitive to mass loss. The equivalent widths of the hydrogen lines are presented in Fig. 8 for the Brackett lines and in Fig. 9 for the Pfund lines. In these figures, the luminosity classes Ia-II are denoted by a square (and plotted slightly to the right of their spectral type); class III by a circle, and classes IV-V by a cross (and plotted slightly to the left of their spectral type). In order to quantify the behaviour of hydrogen lines with spectral type, we assign values to spectral types. Spectral types B0 to B9 are assigned the values 10 to 19. For the B-type dwarfs to giants, a quantitative trend is then derived by fitting the EW versus spectral type with a first-order polynomial of the form $A \times S.T. + B$, where S.T. ranges between 10 and 19 as defined above. This is done for 6 dominant hydrogen lines: Brα, Brβ, Pfγ, Pfδ, Pf(11–5) and Pf(13–5), the results are presented in Table 6. We did not measure Pf(10–5), nor Pf(12–5) as we decided to focus on the behaviour among a wide range of upper levels. Hydrogen lines from higher transitions are too weak to be measured in a significant fraction of our sample. We do not extend the same strategy to O-type stars. Indeed, the extrapolation of the linear trend we apply for B-type stars does not provide a satisfactory fit to the data points for O-type stars. The O-type sample is too small to build a quantitative scheme of spectral classification. Moreover,

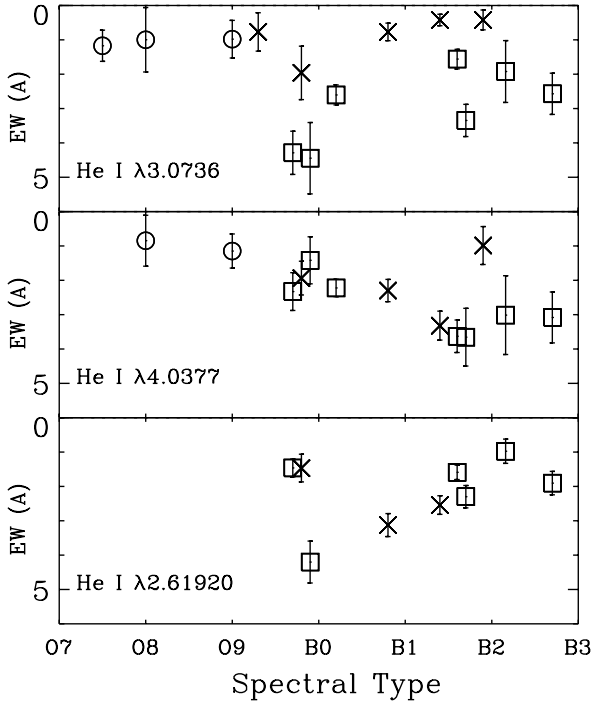

Fig. 10. The equivalent width of three He I lines for normal O and B-type stars. The symbols have identical meaning as in Fig. 8. The λ 3.7036 shows a luminosity-class dependence.

at least one O stars of our sample cannot be part of a general analysis of characteristics of normal early-type stars. Indeed, the O7 V star HD 47839 is a spectroscopic binary. The early B companion affects the spectrum significantly, making the hydrogen lines broader and stronger (Gies et al. 1997). Therefore O-type stars are discussed in a more qualitative way in Sect. 4.3.

4.1. B supergiants and bright giants

Brα is mostly in emission while Brβ is the strongest in absorption of all the hydrogen lines observed, the others getting weaker with higher series and members. The hydrogen lines of B supergiants do not show a significant spectral-type dependence but remain roughly constant, although with a large scatter (see Figs. 8 and 9). This may be related to the variable nature of relatively strong lines in B supergiants. Outward propagating density enhancements (spectroscopically identified as discrete absorption components) and/or modulation of the overall mass-loss rate has been suggested as causes for the time variability of line strength and line shape (see Kaper 1998 for a review). For instance, Kaufer et al. (1996) suggest, on the basis of time-series analysis of Hα in B- and A-type supergiants, that observed variations are due to rotational modulation possibly induced by weak magnetic surface structures, stellar pulsations, and/or instabilities of the ionisation structure of the wind. In dwarf stars, the profiles are predominantly formed in the photosphere where these phenomena are expected to have only a minor impact on the line strength. Therefore, in dwarfs a dependence of line strength on spectral type may be expected (see Sect. 4.2).

Neutral helium lines are detected in O9.5-B3 stars, and can therefore be used to constrain the spectral type to earlier than B3. In the two O supergiants in our sample, the S/N is unfortunately too poor to detect He I. We did not attempt to use the line strength to set the sub-type within O9.5-B3 to avoid over-interpretation. We note that the He I line λ3.0736 μm is found to be systematically stronger in supergiants than in dwarfs stars (cf. Fig. 10).

4.2. B dwarfs and giants

In the B-type dwarfs and giants, all hydrogen lines are seen in absorption, their strengths increasing with later spectral type. This is most pronounced for the lowest Pfund series line observed (Pfγ), and is less so for higher Pfund series lines and Brackett series lines (Table 6). This behaviour suggests that these lines might provide a spectral-type, i.e. temperature diagnostic. All hydrogen lines show a similar first-order dependence, however, the slope for the Brackett lines is smaller than for the Pfund lines.

The most accurate diagnostic for determining the spectral type from the equivalent widths of these lines is to add a number of equivalent widths. Adding all the lines we measured gives the stronger slope, but not the best relation to recover spectral types. Indeed adding the EW of the Pfund lines only, gives the same measure of goodness of fit with smaller errors on the measurements. It is therefore a preferred diagnostic.

We add the EW of the four Pfund lines we measured. The best linear fit relation between spectral type and the summed EW is given in Table 6. Using this relation, we are able to recover the spectral types of all twelve B dwarfs to giants used to define the fit, within two spectral subtypes. Among those, for 8 of the 12 stars we find the spectral type to within one sub-type, and for 6 of the 12 we recover the exact spectral type. This result is quite satisfactory, considering that we adopted a simple linear fit to describe the EW versus spectral-type relation.

The presence of He I lines allows some refinement of our spectral-type estimates, as these lines appear only between spectral type O9 and B2 in dwarfs to giants. This allows us to assign α Pav, which was assigned type B4 considering only the hydrogen lines, its correct spectral type: B2.

Using the summed EW of Brα and Pfγ allows for a linear relation to determine the spectral type, identical to the method described previously. The parameters of this relation are also given in Table 6. The linear fit recovers the spectral type of the 14 B-dwarfs and giants to within five spectral sub-types. Of the 14, for 11 the classification is accurate to within four sub-types; for 10 it is within two sub-types; for 6 it is within one subtype, and for three it is exact. At the extrema of the B classification, B0 and B9, the classification fails by five spectral sub-types, indicating earlier and later spectral types respectively. This suggests

Table 6. Fits giving the relation between spectral type S.T. and EW (in Å) of Brackett and Pfund lines in B-type dwarfs to giants. For zero and first-order polynomials, we give the fit coefficients A (in Å/S.T.) and B (in Å) and their errors, as well as $\sqrt{\chi^2}/N$ as a measure for the goodness of fit (which should be less than about unity). N is the number of stars for which data is available. "All" denotes the sum of all the individual lines given in the table; "Pfund" for the sum of Pfγ, Pfδ, Pf(11-5), and Pf(13-5), and "L'-band" refers to the sum of Brα and Pfγ. The most accurate spectral types may be derived from the "Pfund" lines.

line	A	dA	B	dB	$\sqrt{\chi^2}/N$	N
Brα	–	–	7.93	0.18	0.66	15
	0.41	0.05	1.98	0.79	0.41	15
Brβ	–	–	7.20	0.11	0.74	15
	0.29	0.03	3.11	0.49	0.46	15
Pfγ	–	–	7.21	0.20	0.93	14
	0.65	0.06	−2.23	0.91	0.53	14
Pfδ	–	–	6.29	0.16	0.93	15
	0.65	0.05	−3.03	0.74	0.36	15
Pf(11–5)	–	–	4.78	0.15	0.91	15
	0.57	0.04	−3.48	0.66	0.30	15
Pf(13–5)			3.79	0.15	1.14	13
	0.61	0.05	−5.15	0.72	0.60	13
All			41.53	1.09	0.73	12
	2.84	0.34	−2.00	5.34	0.23	12
Pfund			25.51	0.77	0.82	12
	2.28	0.24	−9.52	3.79	0.23	12
L'-band			15.34	0.38	0.79	14
	1.05	0.11	−0.40	1.71	0.43	14

one must use a higher order fit and/or one has to separate the spectral-type dependence of dwarfs, sub-giants and giants. Unfortunately, the data quality and sample size does not allow us to investigate this possibility. We note that the L'-band spectral range between 3.5 and 4.1 μm also contains some Humphreys series lines. However, these could not be used as their strength can only be accurately measured in late B-type stars.

Given the data quality and spectral coverage of our sample, it is not possible to distinguish between giants and dwarfs using the equivalent widths only. However, the full width at half maximum ($FWHM$) of the Brα line does allow giants and dwarfs to be separated. B-type dwarfs have a $FWHM$ of more than 430 km s^{-1} (up to 665 km s^{-1}), after correction for the instrumental profile, and giants have a $FWHM$ of between 330 and 430 km s^{-1}. Supergiants that show a photospheric profile have even narrower Brα lines. The reason why a simple equivalent width measurement fails to achieve this distinction can be explained by the quality of our data. Indeed, the main source of error in measuring the EW is in the position of the continuum. Assuming Gaussian line shapes, and given our spectral resolution, the relative error in the EW is up to 2.5 times the relative error in the $FWHM$. We also tried to separate giants and dwarfs using the $FWHM$ of Brβ and Pfγ, however, unfortunately without success.

4.3. O stars

Simple relations connecting line strength to spectral type, such as for B dwarfs and giants (see Sect. 4.2), cannot be derived for O-type stars. The reason is a too limited sample of stars that is only observed in the L'-band. The difference in behaviour between Pfγ and Brα also shows that mass loss plays an important role in the line formation process. Pfγ shows a modest dependence of EW on spectral class – dominated by temperature effects, while Brα shows a steep dependence – dominated by wind density effects. In the remainder of this section, we will concentrate on the latter line as a diagnostic for stellar mass loss $\dot{M}$.

All O stars in the sample show emission in Brα, except for two late-type main-sequence stars, i.e. HD 47839 (O7 V) and HD 37468 (O9.5 V). The emission results from the presence of strong stellar winds in these stars (see e.g. Kudritzki & Puls 2000 for a review). This is illustrated in Fig. 11, where the measured Brα equivalent width is plotted versus mass-loss rate. For late O-type stars the Brα equivalent width includes a non-negligible contribution of He I λ4.4049. The $\dot{M}$ values have been determined using either the strength of the Hα profile as a diagnostic or using radio fluxes. Most values are from a compilation by Lamers & Leitherer (1993). Their Hα rates are indicated by square symbols, while diamonds denote radio rates. Three additional measurements (from Puls et al. 1996; Kudritzki et al. 1999) are based on fitting of the Hα line. For three stars (ι Ori, ϵ Ori, and α Cam) multiple mass-loss rate determinations are available. Intrinsic uncertainties in these determinations are typically 0.2–0.3 dex, which is also illustrated by the range in values found for the three stars. The rather large difference in derived mass-loss rate for ι Ori ($\dot{M}$(Hα) = 10.2 × 10^{-7} vs. $\dot{M}$(radio) = 3.2 × 10^{-7} $M_\odot$ yr^{-1}) is likely related to the greater uncertainty in the treatment of the Hα photospheric absorption as well as to the low flux densities at cm wavelengths, for low values of $\dot{M}$. A clear relation between mass-loss rate and Brα equivalent width is present. Adopting an error of 0.2 (0.3) dex in the radio (Hα) rates and applying a weight average for the three stars for which multiple $\dot{M}$ determinations are available, one finds a best fit linear relation:

$$\log \dot{M} = (0.72 \pm 0.21) \log(-W_{\rm eq}{\rm Br}\alpha) - (6.64 \pm 0.28). \quad (1)$$

The most accurate prediction for the mass-loss rate from an equivalent-width measurement is expected if the observed $W_{\rm eq}$ is corrected for photospheric absorption and is plotted versus the equivalent width invariant $Q \equiv \dot{M}^2/(R^{3/2} T_{\rm eff}^2\, v_\infty)$, which is essentially related to the wind density (de Koter et al. 1998; Puls et al. 1996). This method requires accurate basic stellar parameters, which, as pointed out in this paper, are non-trivial to obtain if only infrared data is available. Also, the terminal velocity v_∞ of the stellar wind needs to be known. In O-type stars, this latter quantity is accurately determined from the blue-edge in P Cygni profiles of UV resonance lines.

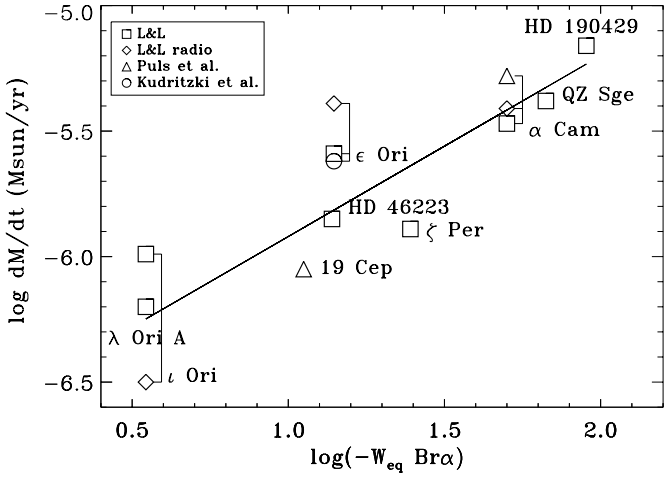

Fig. 11. The measured equivalent width of Brα vs. mass-loss rate as determined from Hα profile fitting and radio measurements. For three stars multiple $\dot{M}$ values are plotted, illustrating the intrinsic uncertainty of mass-loss determination to be ∼0.2–0.3 dex. The adopted values for $\dot{M}$ are from Lamers & Leitherer (1993); Puls et al. (1996), and Kudritzki et al. (1999). All rates are based on Hα fitting, except for three radio determinations (indicated by diamond symbols). See text for a discussion.

If only the near-IR spectrum is observed, such a simple and accurate diagnostic to measure v_∞ is not available. For these reasons, we have opted to provide Eq. (1) as a simple means to obtain an estimate of the stellar mass-loss rate. We note that the relation can equally well be applied to B supergiants, as both for O- and B-type stars the formation of Hα is dominated by the recombination mechanism.

5. B stars with emission lines

In this section, we discuss the B stars with emission lines of our sample, this includes "classical" Be stars as well as B[e] stars and Luminous Blue Variable stars. Some of the spectra presented here have already been studied in great detail, e.g. γ Cas in Hony et al. (2000).

In B stars with emission lines, most hydrogen lines are in emission in the 2.4–4.1 μm range. Those emission lines mainly originate from circumstellar material that are filling in (partially or completely) the atmospheric absorption lines. The nature of the circumstellar material surrounding the objects of this sample is very diverse. In Luminous Blue Variable stars, the emission lines originate from a dense wind. B[e] stars (see Lamers et al. 1999 for a review) have (sometimes strong) forbidden lines implying that there is a large volume of low-density gas near the star in which conditions are favourable for the excitation of these transitions.

It is now well established that "classical" Be stars are surrounded by dense, roughly keplerian circumstellar disks. The most convincing evidence for the presence of disks is derived from direct imaging at optical wavelengths (e.g. Quirrenbach et al. 1997) and at radio wavelengths (Dougherty et al. 1992). Besides imaging, other observed properties of Be stars are also naturally explained by the presence of a circumstellar disk. One of the defining characteristics of Be stars is the presence of (often double-peaked) Hα emission. The width of the Hα line scales with the projected rotational velocity of the photosphere ($v \sin i$) (e.g. Dachs et al. 1986). Both the double-peaked nature and the relation between width and $v \sin i$ are consistent with the line emission being formed in a flattened, rotating disk surrounding the star (Poeckert et al. 1978). In addition, the variations in the violet and red peaks of the Hα and other H I lines in the spectra of Be stars are explained due to spiral density waves in a non-self-gravitating keplerian disk (Telting et al. 1994). Such a keplerian disk geometry also explains the continuum linear polarisation caused by Thomson scattering of free electrons in the disk (e.g. Cote et al. 1987). The position angle of the polarisation is consistent with the orientation of the disk observed by imaging. Be star disks tend to have large densities, as derived from e.g. infrared excess (Waters et al. 1987). The disk radii probably vary from a fraction of a stellar radius (Coté et al. 1996) to many tens of R_* (Waters et al. 1991).

We find no obvious correlation between spectral type and strength of the emission lines in the Be stars with luminosity class III to V (sometimes referred to as classical Be stars) in our sample (Figs. 5 and 6). Other studies report a similar lack of correlation between spectral type and amount of circumstellar gas, except perhaps when it comes to the *maximum* amount of emission at a given spectral type (see e.g. Dougherty et al. 1992 or Waters et al. 1986). We do not see double peaked lines at our resolution ($\delta\lambda/\lambda \approx 1200$). We also do not find evidence for forbidden line emission in the "classical" Be stars, in agreement with such a lack in optical spectra. Further investigation is needed to conclude about the presence of such lines in the spectra of the few B[e] of our sample.

He I emission lines are present in most stars with spectral type earlier than B3. We find a few O I emission lines, the stronger ones being at λ2.8935 and λ3.6617 in several classical Be stars of spectral type earlier than B3 as well as in Luminous Blue Variable stars and in the B[e] star HD 200775. We also find Fe II and Mg II emission lines in all three LBVs. The Fe II lines are also present in the spectra of HD 105435 and HD 45677.

The sample of B stars with emission lines will be investigated in more detail in a forthcoming publication (Lenorzer et al. in prep.).

6. Summary

In this paper, we have presented an atlas of 2.4 to 4.1 μm ISO SWS spectra of early-type stars, mainly obtained during its Post-Helium mission, and several 3.5–4.1 μm spectra of O stars obtained at UKIRT. The observations include normal OB, Be and Luminous Blue Variable stars. Later spectral types will be presented in a separate publication (Vandenbussche et al. in prep.). We have explored

a number of simple empirical methods aimed at using the infrared spectrum to *i)* determine the spectral type and/or luminosity class, and *ii)* determine the mass-loss rate. The main results are:

1. In normal B-type giant to dwarf stars the Pfund lines, and to a lesser extent the Brackett lines, may be used to estimate the spectral type. We provide a simple formula to do this. The leading line of each series shows the most pronounced dependence. Helium lines help to improve this spectral classification, He I being present in late O-type and early B-type stars. All B-type giants and dwarfs have Brα in absorption. The full width at half maximum of this line may be used to discriminate between luminosity classes III and V, the line being broader for dwarfs.

2. In B-type supergiants the equivalent width of all measured hydrogen lines remains constant with spectral sub-type, although with a significant scatter. Brα is seen mostly in emission, while all other lines are in absorption. He I λ3.0736 is systematically stronger in absorption compared to B-type dwarfs and giants.

3. In normal O-type stars and in B-type supergiants, the Brα line is mostly in emission and provides a sensitive indicator of the mass-loss rate. We give a relation that uses the equivalent width of this line to estimate $\dot{M}$.

4. Concerning hydrogen lines, the ones positioned in the L'-band seem best suited to derive physical properties of OB stars when compared to the diagnostics available in other atmospheric bands such as K-, H-, and J-band. The main reason is that the L'-band contains three different hydrogen series lines and includes the leading Brackett-series line. Concerning other species, the K-band seems to contain the most useful lines. This last remark, however, only applies to O-type stars (where e.g. C IV, N III and an unblended He II line are seen) and not to B-type stars which do not show lines of metal species in that wavelength range.

5. In our sample of Be, B[e], and Luminous Blue Variable stars we find no obvious correlation between spectral type and strength of the emission lines. Stars with spectral type earlier than B3 show He I lines, similar to normal B-type stars. Several emission line stars show O I, however not at spectral types later than B2.

Acknowledgements. We thank Jan Cami for stimulating discussions and help in data processing. This work was supported by NWO Pionier grant 600-78-333. AdK kindly acknowledges support from NWO Spinoza grant 08-0 to E. P. J. van den Heuvel. LK is supported by a fellowship of the Royal Academy of Sciences in The Netherlands. TRG is supported by the Gemini Observatory, which is operated by the Association of Universities for Research in Astronomy, Inc., on behalf of the international Gemini partnership of Argentina, Australia, Brazil, Canada, Chile, the UK and the USA. We acknowledge the use of the Atomic Line List compiled by Peter van Hoof, which can be accessed through the web at `http://www.pa.uky.edu/~peter/atomic/index.html`.

Appendix: Equivalent width measurements

The appendix is only available in electronic form at the CDS.

References

Buscombe, W. 1962, Mount Stromlo Obs. Mimeo., 4, 1
Churchwell, E. 1991, NATO ASIC Proc., 342, 221C
Conti, P. S., & Alschuler, W. D. 1971, ApJ, 170, 325
Conti, P. S., & Underhill, A. B. 1988, O Stars and Wolf-Rayet Stars, NASA SP-497
Coté, J., & Waters, L. B. F. M. 1987, A&A, 176, 93
Coté, J., Waters, L. B. F. M., & Marlborough, J. M. 1996, A&A, 307, 184
Dachs, J., Hanuschik, R., & Kaiser, D. 1986, A&A, 159, 276
Decin, L. 2000, Ph.D. Thesis, Katholieke Universiteit Leuven, Belgium
Dougherty, S. M., & Taylor, A. R. 1992, Nature, 359, 808
Gies, D. R., Mason, B. D., Bagnuolo, W. G., et al. 1997, ApJ, 475, L49
de Graauw, T., Haser, L. N., Beintema, D. A., et al. 1996, A&A, 315, L49
Guetter, H. H. 1968, PASP, 80, 197
Hanson, M. M., Conti, P. S., & Rieke, M. J. 1996, ApJS, 107, 281
Hanson, M. M., Rieke, M. J., & Luhman, K. L. 1998, ApJ, 116, 1915
Hiltner, W. A., Garrison, R. F., & Schild, R. E. 1969, ApJ, 157, 313
Hony, S., Waters, L. B. F. M., Zaal, P. A., et al. 2000, A&A, 355, 187
Houk, N. 1975, Michigan Spectral Survey, 1
Houk, N. 1982, Michigan Spectral Survey, 3
Houk, N., & Smith-Moore, M. 1988, Michigan Spectral Survey, 4
van der Hucht, K. A., Morris, P. W., Williams, P. M., et al. 1996, A&A, 315, 193
Humphreys, R. M., & Davidson, K. 1994, PASP, 106, 1025
Johnson, H. L., & Morgan, W. W. 1953, ApJ, 117, 313
Kaper, L. 1998, ESASP, 413, 149
Kaufer, A., Stahl, O., Wolf, B., et al. 1996, A&A, 314, 599
Kessler, M. F., Steinz, J. A., Anderegg, M. E., et al. 1996, A&A, 315, L27
de Koter, A., Heap, S. R., & Hubeny, I. 1998, ApJ, 509, 879
Kudritzki, R.-P., Puls, J., & Lennon, D. J. 1999, A&A, 350, 970
Kudritzki, R.-P., & Puls, J. 2000, ARA&A, 38, 613
Lamers, H. J. G. L. M., & Leitherer, C. 1993, ApJ, 412, 771
Lamers, H. J. G. L. M, Morris, P. W., Voors, R. H. M., et al. 1996a, A&A, 315, 225
Lamers, H. J. G. L. M, Najarro, F., Kudritzki, R. P., et al. 1996b, A&A, 315, 229
Lamers, H. J. G. L. M., Zickgraf, F. J., de Winter, D., et al. 1999, A&A, 340, 117

Lennon, D. J., Dufton, P. L., & Fitzsimmons, A. 1992, A&AS, 94, 569
Lesh, J. R. 1968, ApJS, 17, 371
Levato, H. 1975, A&AS, 19, 91
Lorente, R. 1998, in the ISO Handbook, vol. VI, http://www.iso.vilspa.esa.es/users/expl_lib/expl_lib.html
Massey, P., & Thompson, A. B. 1991, AJ, 101, 1408
Meyer, M. R., Edwards, S., Hinkle, K. H., & Strom, S. E. 1998, ApJ, 508, 397
Morgan, W. W., Code, A. D., & Withford, A. E. 1955, ApJS, 2, 41
Morgan, W. W., & Keenan, P. C. 1973, ARA&A, 11, 29
Morris, P. W., Eenens, P. R. J., Hanson, M. M., Conti, P. S., & Blum, R. D. 1996, ApJ, 470, 597
Morris, P. W., van der Hucht, K. A., Willis, A. J., & Williams, P. M. 1997, Ap&SS, 255, 157
Morris, P. W., van der Hucht, K. A., Crowther, P. A., et al. 2000, A&A, 353, 624
Mountain, C. M., Robertson, D. J., Lee, T. J., et al. 1990, SPIE, 1235, 25
van Paradijs, J. 1994, ASP Conf. Ser., 56, 165
Poeckert, R., & Marlborough, J. M. 1978, ApJS, 38, 229
Puls, J., Kudritzki, R.-P., Herrero, A., et al. 1996, A&A, 305, 171
Quirrenbach, A., Bjorkman, K. S., & Bjorkman, J. E., et al. 1997, ApJ, 479, 477
Smith, L. F., Shara, M. M., & Moffatt, A. F. J. 1996, MNRAS, 281, 163
Telting, J. H., Heemskerk, M. H. M., Henrichs, H. F., et al. 1994, A&A, 288, 558
Vandenbussche, B., Waters, L. B. F. M., de Graauw, T., et al. 2000, ESASP, 456, 147
Walborn, N. R. 1972, AJ, 77, 312
Walborn, N. R. 1973, AJ, 78, 1067
Walborn, N. R., & Fitzpatrick, E. L. 1990, PASP, 102, 379
Wallace, L., Meyer, M. R., Hinkle, K., & Edwards, S. 2000, ApJ, 535, 325
Waters, L. B. F. M., Coté, J., & Lamers, H. J. G. L. M. 1987, A&A, 185, 206
Waters, L. B. F. M., Marlborough, J. M., van der Veen, W. E. C., et al. 1991, A&A, 244, 120
Zorec, J., Moujtahid, A., Ballereau, D., et al. 1998, ASSL, 233, 55